American Institute of Aeronautics and Astronautics

AIAA 2004-0764

Experimental and Computational Evaluation of Flush-Mounted, S-Duct Inlets (Invited)

Bobby L. Berrier
Brian G. Allan
NASA Langley Research Center
Hampton, Virginia, U.S.A.

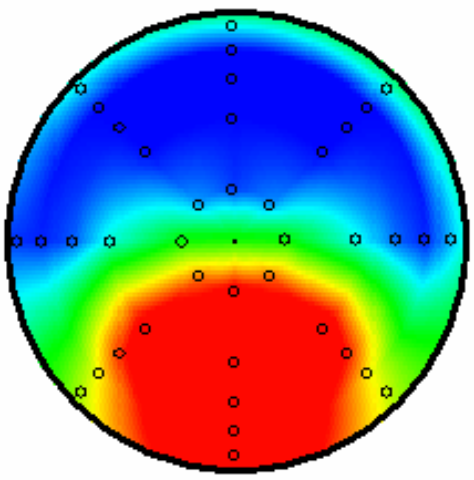

42nd AIAA Aerospace Sciences Meeting & Exhibit
5-8 January 2004
Reno, Nevada

Experimental and Computational Evaluation of Flush-Mounted, S-Duct Inlets

Bobby L. Berrier* and Brian G. Allan†
NASA Langley Research Center
Hampton, Virginia 23681-2199

ABSTRACT

A new high Reynolds number test capability for boundary layer ingesting inlets has been developed for the NASA Langley Research Center 0.3-Meter Transonic Cryogenic Tunnel. Using this new capability, an experimental investigation of four S-duct inlet configurations was conducted. A computational study of one of the inlets was also conducted using a Navier-Stokes solver. The objectives of this investigation were to 1) develop a new high Reynolds number inlet test capability for flush-mounted inlets, 2) provide a database for CFD tool validation, 3) evaluate the performance of S-duct inlets with large amounts of boundary layer ingestion and 4) provide a baseline inlet for future inlet flow-control studies. Tests were conducted at Mach numbers from 0.25 to 0.83, Reynolds numbers (based on duct exit diameter) from 5.1 million to a full-scale value of 13.9 million, and inlet mass-flow ratios from 0.39 to 1.58 depending on Mach number. Results of the experimental study indicate that inlet pressure recovery generally decreased and inlet distortion generally increased with increasing Mach number. Except at low Mach numbers, increasing inlet mass-flow increased pressure recovery and increased distortion. Increasing the amount of boundary layer ingestion or ingesting a boundary layer with a distorted profile decreased pressure recovery and increased distortion. Finally, increasing Reynolds number had almost no effect on inlet distortion but increased inlet recovery by about one-half percent at a Mach number near cruise. The computational results captured the inlet pressure recovery and distortion trends with Mach number and inlet mass-flow well; the reversal of the pressure recovery trend with increasing inlet mass-flow at low and high Mach numbers was predicted by CFD. However, CFD results were generally more pessimistic (larger losses) than measured experimentally.

SYMBOLS

AIP	Aerodynamic Interface Plane
A_h	inlet highlight area, ft^2
A_i	inlet throat area, ft^2
A0AH	Inlet mass-flow ratio
A_2	diffuser exit (fan face) area, ft^2
a	inlet lip length (longitudinal distance between highlight and throat), ft
BLI	Boundary Layer Ingesting (or Ingestion)
BWB	Blended Wing Body
b	inlet lip height (vertical distance between highlight and throat), ft
	$DPCP_{avg}$ average SAE circumferential distortion descriptor
CFD	Computational Fluid Dynamics
$DPRP_{max}$	maximum SAE radial distortion descriptor
D_2	diffuser exit (fan face) diameter, ft
H_i	inlet throat height, ft
ΔH	inlet offset (vertical distance between throat centroid and exit centroid), ft
L	inlet diffuser length (longitudinal distance from throat to exit), ft
M	free-stream Mach number
PAV_i	average total pressure of ring i, psi
$PAVLOW_i$	average total pressure of low total-pressure region for ring i, psi
P_{TBL}	boundary layer rake total pressure, psi
P_{T0}	free-stream total pressure, psi
P_{T2}/P_{T0}	pressure recovery
P_{T2}	average AIP total pressure, psi
Re_{D2}	Reynolds number based on diameter of AIP
Re/ft	Reynolds number per foot
T_{T0}	free-stream total temperature, °F
W_i	inlet throat width, ft
W2C	AIP full-scale corrected mass-flow rate, lbm/s
z	distance above tunnel wall, ft
δ	tunnel wall boundary layer thickness at inlet face, ft

INTRODUCTION

Highly integrated boundary layer ingesting (BLI), offset or S-duct aircraft inlets have the potential benefits of reduced drag, size and weight by eliminating

---

* Fellow AIAA, Associate Branch Head
† Member AIAA, Aerospace Engineer

the boundary layer diverter and shortening the inlet duct; reduced ram drag by reducing the momentum of the inlet flow[1]; and lower observability. However, to obtain these benefits from a system level requires that high pressure recovery and acceptable distortion levels be maintained for engine operation. The use of S-duct inlets is not new, even for commercial vehicles. The Boeing 727[2] and Lockheed L-1011 successfully utilized offset or S-duct inlet designs. In addition, as many new military aircraft have diverterless S-duct inlet systems, design issues have obviously been solved when the inlet is integrated on the forward portion of the vehicle with small boundary layer heights to ingest. Design guidelines for S-duct diffusers without significant amounts of BLI seem to be well understood.[3,4]

However, design issues become somewhat more intractable when the inlet is integrated on the aft portion of the vehicle. The early Blended-Wing-Body (BWB) transport configuration[5,6] with either a single mail-slot inlet or individual flush-mounted inlets is an example of this type of inlet integration. The BWB has approximately a 25 in. thick boundary layer near the wing/body trailing edge which is about 25-30% of the inlet height for a flush-mounted inlet on this configuration. Although this amount of BLI may be a formidable challenge, several unpublished studies have indicated large benefits for BLI (up to 10% reduction in fuel burn for example) if this problem can be solved.

Two of the major technical challenges that must be addressed for BLI, S-duct inlets integrated on the aft portion of the vehicle are the complex inlet aerodynamics and the nonuniform engine-face flow distribution. The complex inlet aerodynamics are driven by thick, degraded boundary layers approaching the inlet, wing/body shocks at transonic speeds, and adverse pressure gradients caused by wing/body closure and inlet blockage. Nonuniform engine face pressure distributions are driven by S-duct diffuser effects (secondary- or cross-flows for example), ingested low momentum boundary layer flow, and internal flow separation. Failure to adequately resolve these issues will result in low inlet pressure recovery and high inlet pressure distortion thus reducing available thrust and engine operability and possibly wiping out the benefits realized from the configuration design.

A search of open literature revealed no experimental information on BLI S-duct inlet performance for inlets with large amounts of BLI operating at realistic conditions. Most BLI investigations reported in the literature either considered only small amounts of BLI (boundary layer thickness on the order of 10% inlet diameter) or were conducted at extremely low Mach and Reynolds numbers.[7,8,9,10] The objectives of the current study were to develop a new high Reynolds number inlet test capability for BLI inlets; evaluate the performance of S-duct inlets with large amounts of BLI (boundary layer thickness up to 30% of inlet height) at realistic operating conditions (high subsonic Mach numbers and full-scale Reynolds numbers); provide a database for CFD tool validation; and provide a baseline inlet for future inlet flow-control studies.

EXPERIMENTAL APPARATUS AND METHODS

Facility

An experimental evaluation of four BLI S-duct inlets was conducted in the NASA Langley Research Center 0.3-Meter Transonic Cryogenic Tunnel[11,12] at realistic operating conditions (Mach, Reynolds number and inlet mass-flow). This facility is a closed loop, fan driven tunnel with a 13- by 13-inch test cross section. The normal test medium is gaseous nitrogen which is injected as a cryogenic liquid that allows operating temperatures down to –320 °F. It has a Mach range of 0.1 to 0.9 and a total pressure range from atmosphere to 88 psi. Utilizing the facility variable total pressure and total temperature capabilities, Reynolds numbers up to 100 million per foot can be obtained.

Model

In a contracted effort, four inlets were designed by the Boeing Company to fit in the design space of both BWB transport and military aircraft applications. The four inlet designs (two different throat aperture aspect ratios of 0.95 and 1.42 with two inlet lip thicknesses, a/b = 2.0 and 3.0, for each) are shown in figure 1 and are characterized by the geometry shown in Table 1. The semi-elliptical aperture was intended to potentially provide a favorable pressure field of the upper diffuser wall upon the lower diffuser wall. The thinner internal cowl forebody shape (a/b = 3.0) was intended to provide better performance at $M > 0.83$ than the thicker shape (a/b = 2.0).

The tunnel wall boundary layer was used to simulate the boundary layer ingested by a BWB transport inlet (approximately 30% BLI). Since the facility boundary layer was not adjustable, estimated wall natural boundary layer height set the inlet scale at 2.5% to represent potential BWB transport inlet designs with $\delta/H_i = 0.278$ (semi-circular inlets) and 0.331 (semi-elliptical inlets). The actual boundary layer height measured during the test was about 30 percent larger than the estimated height and resulted in the nominal δ/H_i values shown in table 1. In an attempt to determine the impact of a different boundary layer

profile on inlet performance, two "fences" fabricated from small gage wire were tested installed in front of inlet configuration A.

All four models share the same diffuser centerline distribution; inlet configurations A and B share a common diffuser design and inlet configurations C and D also are share a common diffuser design. Geometric inlet area, which is larger than A_i, was designed to accommodate the ingested boundary layer by accounting for boundary layer displacement thickness. Finally, Gerlach shaping was utilized in the design of the diffuser cross sections to help control secondary flows in the diffuser.

A new tunnel sidewall was designed and fabricated such that the inlet models could be flush mounted directly on the wall. Figure 2 presents a photograph showing the inlet model mounted on the new sidewall. The inlet S-duct diffuser extended through the wall into the wind-tunnel plenum. A photograph showing the back (plenum) side of the inlet installation is shown in figure 3. The outer wind-tunnel plenum wall was removed for this photograph. At the diffuser exit, the inlet flow enters an Aerodynamic Interface Plane (AIP) instrumentation section with a fan face total pressure rake and is then ducted through a mass-flow plug assembly. The mass-flow plug assembly includes pressure and temperature instrumentation and a calibrated bellmouth/plug combination that provided inlet airflow as a function of plug position and pressure. The motor that drove the variable position plug was housed in an insulated and heated motor box. The inlet flow was then ducted outside the wind tunnel and vented to atmosphere. Unlike many inlet models, the current inlet models depended on the pressure differential between tunnel total-pressure and atmospheric-pressure to drive the inlet flow and did not have a separate ejector system used for this purpose.

Instrumentation

Inlet diffuser instrumentation consisted of 74 static pressure orifices (30 each on the upper and lower wall centerlines and 7 each on each sidewall). To obtain inlet pressure recovery and distortion parameters, a 40-probe total pressure rake with 8 arms (located 45° apart) and 5 instrumentation rings (5 probes on each arm) was located at the AIP (duct exit). This rake can be seen in the photograph of figure 2. In addition to the 40 steady state total pressures, 3 dynamic pressure measurements were made on the bottom (180°) arm of the rake. They were placed on this arm since it was expected that BLI and duct secondary flow effects would be most severe at the bottom of the duct. Instrumentation in the flow-plug assembly included 3 rakes located 120° apart that measured 5 total pressures, 1 static pressure, and 1 total temperature at each rake position; 3 rings of 3 static pressures each located in the bellmouth wall; and a potentiometer that measured plug position. Wind tunnel wall boundary layer was measured with an 8-probe boundary layer rake located beside the inlet at the nominal inlet highlight plane. Because one of the test objectives was to obtain data for CFD code validation, the wind tunnel walls were also instrumented with 51 static pressure orifices in the left-hand sidewall (side with inlet installation), 40 static pressure orifices in the right-hand wall, and 18 static pressure orifices in both the ceiling and floor.

Data Reduction

The primary inlet performance parameters used in this paper are inlet pressure recovery, P_{T2}/P_{T0} and average SAE circumferential distortion descriptor, $DPCP_{avg}$. The SAE distortion descriptor had all empirical sensitivity constants set to 1.0 and offset terms set to 0.0.[13] In this form, $DPCP_{avg}$ is equal to the average distortion intensity and is defined by equation (1).

$$DPCP_{avg} = Intensity_{avg} = \sum_{i=1}^{i=5} \frac{Intensity_i}{5}, \qquad (1a)$$

$$\text{where } Intensity_i = \frac{PAV_i - PAVLOW_i}{PAV_i} \qquad (1b)$$

and i = ring number on the AIP rake.

Inlet pressure recovery is defined by equation (2).

$$P_{T2}/P_{T0} = \text{Average AIP rake total pressure}/P_{T0} \qquad (2)$$

Test Conditions

One of the test objectives was to evaluate the performance of S-duct inlets with large amounts of BLI (see Table 1) at realistic operating conditions (high subsonic Mach numbers and full-scale Reynolds numbers). A nominal full-scale Reynolds number (based on engine diameter) for a notional BWB transport aircraft is 13.9×10^6 at M = 0.85 and 39,000 feet altitude. The nominal test conditions for the current study are given in Table 2.

Since the model was attached to the tunnel sidewall, angle-of-attack and beta were fixed at a value of zero-degrees. Because the facility adaptive wall capability was inoperable at the time of this study, the walls were locked in a fixed position and the maximum Mach number that could be tested was M = 0.83. A

Reynolds number sweep was conducted at M = 0.83 and a Reynolds number per foot of 42 x 10^6 was tested at two different combinations of tunnel total temperature and total pressure. Inlet mass-flow was varied by changing plug position relative to a bellmouth; the A0AH and $W2C/A_i$ values shown in Table 2 are nominal measured values. The maximum design value (top of climb) of $W2C/A_i$ was about 42.8 lbm/s·ft^2 (cruise would be less); because of the larger than estimated boundary layer thickness on the tunnel wall mentioned previously, the inlet throat was undersized and the actual maximum airflow value obtained was less as shown in Table 2.

COMPUTATIONAL METHOD

Numerical Modeling

Numerical simulations were performed using OVERFLOW, a flow solver code developed at NASA.[14,15] OVERFLOW solves the compressible Reynolds averaged Navier-Stokes (RANS) flow equations using a finite-difference formulation. For this investigation the steady-state RANS equations were solved on structured grids using an overset grid framework. Turbulence was modeled using the two-equation Shear Stress Transport (SST) model implemented by Menter.[16]

The inlet flow was simulated using the inlet A model mounted on a flat plate surface where the upper and side walls of the wind tunnel were not modeled. The boundary layer height was set to match the experiment by varying the length of the flat plate ahead of the inlet. The mass flow rate for the inlet was set to match the experiment by varying the downstream exit pressure inside of the inlet.

Grid

The external and internal flows were modeled using seven overset structured grids having a total of 4.2 million grid points. Figure 4 shows the symmetry plane depicting the external and internal flow regions. Figure 5 shows a view of the surface grids and the overlapped grid regions. The overset grids were generated using the Chimera Grid Tools software developed at NASA.[17] The domain connectivity between the overlapped regions was computed using the PEGASUS.[18]

RESULTS

Effect of Mach Number and Airflow

Inlets for subsonic podded nacelles typically have pressure recovery of 0.98 or better. Any pressure recovery losses incurred for this inlet type are dominated by friction drag and lip separation (only at off-design conditions). It is not unusual to assume perfect recovery (P_{T2}/P_{T0} = 1.0) during aircraft conceptual design for these type inlets.[19]

For BLI S-duct inlets, duct curvature and boundary layer ingestion introduces additional losses to inlet pressure recovery performance. The first bend in an S-duct inlet causes a top-to-bottom pressure differential that creates secondary flows along the duct wall[8,20]; this secondary flow tends to migrate the wall boundary layer toward the low pressure side of the bend (lower wall for current investigation). If sufficient boundary layer is accumulated, it produces a lift-off effect or separation of the inlet core flow. Although it might be expected that the second bend in an S-duct would reverse or mitigate this effect, studies have indicated that this is not the case. The S-duct P_{T2}/P_{T0} penalty relative to a straight duct is about 2 percent.[8,19] An additional pressure recovery penalty is incurred because of the large amount of boundary layer ingestion for the current model (Nominal δ/H_i = 0.36 to 0.43 for current inlets; see Table 1). Increasing ingested boundary layer thickness to nominal δ/H_i values of about 0.1 to 0.2 (significantly less δ/H_i than current inlets) causes about a 2 percent penalty.[10,21]

Inlet performance derived from the experimental and computational studies of Inlet A is presented in figures 6 and 7. Total-pressure ratio contour maps at the AIP (fan face) are presented in figure 6 for various test conditions; pressure recovery (P_{T2}/P_{T0}) and circumferential distortion ($DPCP_{avg}$) trends with Mach number and inlet airflow are presented in figure 7. The experimental trends indicated in these figures are typical for all four inlet configurations tested.

Qualitatively, the experimental and computational studies give similar results as shown in figure 6. Both show large areas of low total pressure near the lower duct wall at M = 0.83. As discussed previously, these low pressure regions are caused by the ingestion of low energy boundary layer flow (BLI) and secondary duct flow effects induced by the S-duct inlet geometry and would result in reduced inlet pressure recovery and increased inlet distortion. Both studies also indicate that the low-pressure regions grow in size and intensity at M = 0.83 with increasing inlet airflow. Some flow asymmetry can be noted in the experimental contour map at M = 0.83, $W2C/A_i$ = 36.8 lbm/s·ft^2; such flow asymmetries are not captured by the CFD since the geometry and flow conditions are assumed to be left/right symmetrical. Finally, the computational results produce a larger low-pressure area than

measured experimentally at all four test conditions shown; this result would cause the CFD performance to be more pessimistic than the experimental performance.

The effects of Mach number and inlet airflow on pressure recovery, P_{T2}/P_{T0}, are shown in the upper portion of figure 7. Increasing Mach number resulted in very large reductions in inlet pressure recovery. This trend with Mach number is typical of most inlets but the losses are exaggerated by the S-duct inlet shape and the large amount of boundary layer ingestion. The losses are larger than those reported from previous investigations of BLI. At M = 0.25 where losses less than 1-percent were measured, the pressure recovery loss is primarily caused by friction on the duct wall and some small BLI effects (note the total-pressure-ratio contour maps at M = 0.25 in figure 6). As indicated by the total-pressure-ratio contour plots at M = 0.83 in figure 6 that show a large low-pressure region near the bottom duct wall (particularly at high airflow rates near cruise), pressure recovery losses at high Mach numbers is dominated by duct curvature and BLI effects and, as shown in figure 7, pressure recovery losses of over 4-percent were measured. As will be shown later, pressure recovery losses of over 6-percent were measured for some of the inlets of the current study. Pressure recovery losses of 4- to 6-percent could be devastating to engine performance and commercial viability of a BLI transport concept; future research into methods for mitigating duct curvature and BLI losses is required.

As indicated in figure 7, inlet pressure recovery is also a function of inlet airflow. At M = 0.25, where duct curvature and BLI effects are very small, pressure recovery decreases slightly with increasing airflow while at M > 0.4, pressure recovery increases with increasing airflow.

At low Mach numbers and low throttle or airflow settings, the inlet is able to meet airflow requirements with very small losses (basically friction) and thus pressure recovery is high. However, at high throttle settings, the inlet throat area is too small and the inlet must "suck" air into the duct from the surrounding flow field (stream tube larger than inlet area). This may not only create larger lip losses (internal lip separation can occur in the extreme case) but also "suck" additional boundary layer into the duct from the inlet sides and thus lower pressure recovery. Although not shown herein, this effect was more pronounced for Inlets C and D that had larger initial amounts of BLI.[22]

At high subsonic speeds, the inlet is operating near design and pressure recovery losses will be dominated by duct curvature and BLI effects. Since the percentage of BLI relative to total airflow decreases with increasing airflow (the amount of BLI will remain nearly constant), the pressure recovery losses decrease and pressure recovery increases with increasing airflow at high subsonic speeds.

Computational pressure recovery results are shown in figure 7 by solid symbols. The four CFD data points correspond to the four total-pressure contour maps shown in figure 6. Although the CFD results are generally slightly pessimistic (indicate larger pressure recovery losses), the trends with increasing Mach number and inlet airflow are well predicted. The reversal in the trend with increasing inlet airflow at M = 0.25 and M = 0.83 is captured by CFD.

The effect on Mach number and inlet airflow on the SAE circumferential distortion descriptor is shown on the bottom portion of figure 7. Acceptable static distortion levels are generally considered to be below a range from 0.04 to 0.05. Based on this level, the distortion levels shown in figure 7 are marginal at Mach numbers and airflows near cruise. This result indicates that some form of flow control could be beneficial for the inlets of this study. Inlet distortion generally increased with increasing Mach number and increasing airflow for the inlets of this study (particularly for M > 0.4). This result is vividly illustrated by comparing the total-pressure-ratio contour plots provided in figure 7. It should be noted that although increased airflow was beneficial to pressure recovery at M > 0.4, the opposite was generally true for distortion over the same Mach range. Although CFD results for distortion (solid symbols) were again generally pessimistic, especially at the higher Mach number, distortion trends with increasing Mach number and inlet airflow were well predicted by CFD.

Effect of Inlet Aperture Geometry

Four inlet aperture configurations, two aperture shapes (semi-circular and semi-elliptical) with two lip thicknesses each, were tested in the current investigation (see figure 1 and Table 1). The semi-circular shape is similar to the BWB BLI inlet design.[5,6,8] The semi-elliptical shape was included to 1) take advantage of a potentially favorable pressure field of the upper diffuser wall upon the lower diffuser wall and thus weaken internal secondary flows, and 2) increase the amount of boundary later ingested and thus take advantage of potential BLI benefits[1] (note that these benefits are not addressed in the current investigation). The a/b = 2.0 inlet lip was designed for cruise conditions between 0.77 < M < 0.83 and the a/b = 3.0 inlet lip was designed for cruise at M > 0.83. Figure 8 presents a comparison of inlet performance for these configurations as a function of Mach number at

two airflow values. At M > 0.4, the semi-circular aperture shape (Inlets A and B) produced lower distortion and higher pressure recovery than the semi-elliptical aperture shape (Inlets C and D). For a given inlet throat area, the semi-elliptical inlet will ingest more boundary layer than the semi-circular inlet because it is wider than and not as high as the semi-circular inlet. This results in an increase in measured nominal δ/H_i from 0.358 for the semi-circular inlets to 0.434 for the semi-elliptical inlets. If the semi-elliptical shape produced any favorable effects on internal duct secondary flows, they were more than offset by the detrimental effects of BLI discussed previously for figure 7. This means that the detrimental BLI effects on inlet performance must either be alleviated by new flow control technologies or that any potential vehicle performance BLI benefits[1] must offset the detrimental effects on inlet performance in order for BLI inlets to be a viable concept.

In general, inlet lip thickness only had a small effect on inlet performance. As might be expected, a thicker lip improved pressure recovery of the semi-circular inlet configuration at low speeds (comparison data not obtained at the low speed, high-airflow rate) but a similar improvement was not measured for the semi-elliptical inlet. As mentioned previously, the facility adaptive wall capability was inoperable at the time of this study and Mach numbers above 0.83 could not be obtained. Thus, the potential benefits of a sharp inlet lip at M > 0.83 could not be verified. It appears that there is a cross-over in inlet distortion at M = 0.83, but higher Mach test data are needed to verify that this benefit of a sharper inlet exists at higher speeds.

Effect of Reynolds Number

Using the variable temperature and pressure capability of the 0.3-Meter Transonic Cryogenic Tunnel[11,12], a Reynolds number sweep was conducted at M = 0.83. As shown in Table 2, Reynolds number per foot was varied from 25×10^6 to 68×10^6 (full scale for the notional BWB aircraft). The effect of Reynolds number on the performance of Inlet A (semi-circular aperture) and Inlet C (semi-elliptical aperture) is presented in figure 9 as a function of airflow at a Mach number of 0.83. Although the effect is small (less than one half percent), increasing Reynolds number increased inlet pressure recovery. Based on measured boundary layer thicknesses, this improvement in pressure recovery cannot be attributed to a Reynolds number effect on boundary layer thickness or amount of BLI. Thus, by elimination, the pressure recovery improvement must be associated with an improvement in the internal duct flow characteristics such as secondary flow and/or separation. As indicated at the bottom of figure 9, Reynolds number has a negligible effect on the inlet circumferential distortion descriptor. There is a very slight tendency for distortion to be reduced by increasing Reynolds number at the very highest airflow tested.

Effect of Boundary Layer Profile

The measured shape factor of the natural wall boundary layer in the 0.3-Meter Transonic Cryogenic Tunnel at the inlet face plane was about 1.49. In flight, the boundary layer entrance profile can be quite different from that created on a wind tunnel facility wall because of other factors – shock-boundary layer interaction ahead of the diffuser for example. To obtain a measure of inlet performance sensitivity to boundary layer profile, Inlet A was tested with two fences installed in front of the inlet face. A photograph of the fence installation is shown on the top-left of figure 10. Utilizing upstream devices such as chains, fences and backward steps to perturb boundary layer profile has been used in several previous investigations.[7,8,10] The effects of fence installation on boundary layer profile and inlet performance of Inlet A from the current investigation are shown in figure 10. It should be noted that at some unknown time during the fence-on testing, a portion of the fence wires broke and were lost downstream. However, the boundary layer profile shown on the upper-right portion of figure 10 was measured simultaneously with the performance data shown at M = 0.6.

The effect of a distorted boundary layer profile on the performance of Inlet A at $W2C/A_i$ = 31 lbm/s·ft^2 is shown on the lower half of figure 10 as a function of Mach number. Distortion of the boundary layer profile was detrimental to both inlet distortion and pressure recovery. The result shown in figure 10 for the effect of a distorted boundary layer profile on pressure recovery is almost identical to that measured in a previous study.[10] This study, which utilized a backward step to perturb the boundary layer, measured a 0.0071 reduction in pressure recovery at a throat Mach number of 0.7 as a result of distorting the entrance profile; the current investigation resulted in a 0.0058 reduction in pressure recovery at a free-stream Mach number of 0.6 as a result of distorting the entrance profile. However, an opposite trend on inlet distortion was measured in the current investigation from that reported in reference 10. In reference 10, although a thick boundary layer and a thick boundary layer with distorted entrance profile both caused higher distortion than a thin boundary layer, perturbing the thick boundary layer

actually reduced inlet distortion from that produced by the unperturbed thick boundary layer. In the current investigation, perturbing the entrance profile of a thick boundary layer (significantly thicker than that reported in reference 10) increased inlet distortion. Although the fences used during the current investigation may not produce a realistic entrance boundary layer profile, the results make it clear that inlet performance is not only a function of the amount of BLI but also a function of boundary layer health (shape factor) and upstream disturbances.

CONCLUSIONS

A new high Reynolds number test capability for boundary layer ingesting inlets has been developed for the NASA Langley Research Center 0.3-Meter Transonic Cryogenic Tunnel. Using this new capability, an experimental investigation of four S-duct inlet configurations with large amounts of boundary layer ingestion (nominal boundary layer thickness of about 40% of inlet height) was conducted at realistic operating conditions (high subsonic Mach numbers and full-scale Reynolds numbers). A computational study of one of the inlets was also conducted. The results from this investigation have indicated the following conclusions.

1. Ingestion of a large amount of boundary layer into an S-duct inlet causes a significant decrease in inlet pressure recovery on top of losses associated with duct friction, inlet lip separation, or duct curvature.

2. Increasing free-stream Mach number was generally detrimental to boundary layer ingesting (BLI) S-duct inlet performance (pressure recovery and distortion). The losses at high subsonic speeds are dominated by duct curvature and BLI effects.

3. Increasing inlet airflow (engine throttle setting) increased inlet pressure recovery at Mach numbers above 0.4 but also increased inlet distortion. The increase in pressure recovery is attributable to a reduction in the relative amount of BLI as inlet mass-flow is increased.

4. At a Mach number of 0.25, increasing engine throttle setting decreased inlet pressure recovery. At this speed, the inlet mass-flow ratio is generally greater than 1.0 (inlet stream tube is larger than inlet throat area) and amount of boundary layer is “sucked” into the inlet increases with increasing engine throttle setting.

5. Because of increased BLI, BLI inlets with semi-elliptical apertures have lower inlet performance (lower pressure recovery and higher distortion) than inlets with semi-circular apertures. Inlet lip thickness had only a small effect on inlet performance for the range of variables tested.

6. Increasing Reynolds number had a negligible effect on inlet distortion but increased inlet pressure recovery.

7. Distorting the boundary layer entrance profile reduced inlet performance of the BLI S-duct inlets of the current investigation.

8. Because of the impact of Reynolds number and boundary layer entrance profile on inlet performance, it is important that future investigations on BLI S-duct inlet configurations be conducted at as realistic test conditions as possible.

9. CFD was able to capture the inlet pressure recovery and distortion trends with increasing Mach number and inlet mass-flow; the reversal of the pressure recovery trend with increasing inlet mass-flow at low and high Mach numbers was predicted by CFD. However, CFD results were generally more pessimistic (larger losses) than measured experimentally.

REFERENCES

1. Smith, Leroy H.: Wake Ingestion Propulsion Benefit. Journal of Aircraft and Power, Vol. 9, No. 1, Jan.-Feb., 1993.

2. Ting, C.T.; Kaldschmidt, G.; and Syltebo, B.E.: Design and Testing of New Center Inlet and S-Duct for B-727 Airplane With Refanned JT8D Engines. AIAA Paper 75-0059, Jan., 1975.

3. Mayer, David W.; Anderson, Bernhard H.; and Johnson, Timothy A.: 3D Subsonic Diffuser Design and Analysis. AIAA 98-3418, 1998.

4. Tindell, R.H.: Highly Compact Inlet Diffuser Technology. AIAA-87-1747, July, 1987.

5. Liebeck, R.H.; Page, M.A.; and Rawdon, B.K.: Blended-Wing-Body Subsonic Commercial Transport. AIAA 98-0438, Jan. 1998.

6. Roman, D.; Allen, J.B.; and Liebeck, R.H.: Aerodynamic Design Challenges of the Blended-Wing-Body Subsonic Transport. AIAA-2000-4335, 2000.

7. Anabtawi, Amer J.; Blackwelder, Ron; Liebeck, Robert; and Lissaman, Peter: Experimental Investigation of Boundary Layer Ingesting Diffusers of a Semi-Circular Cross Section. AIAA-98-0945, 1998.

8. Anabtawi, Amer J.; Blackwelder, Ron F.; Lissaman, Peter B.S.; and Liebeck, Robert H.: An Experimental Investigation of Boundary Layer Ingestion in a Diffusing S-Duct With and Without Passive Flow Control. AIAA 99-0739, 1999.

9. Anabtawi, Amer J.; Blackwelder, Ron F.; Liebeck, Robert H.; and Lissaman, Peter B.S.: An Experimental Study of the Effect of Offset on Thick Boundary Layers Flowing Inside Diffusing Ducts. AIAA 99-3590, 1999.

10. Ball, W.H.: Tests of Wall Blowing Concepts for Diffuser Boundary Layer Control. AIAA-84-1276, 1984.

11. Mineck, Raymond E.; and Hill, Acquilla S.: Calibration of the 13- by 13-Inch Adaptive Wall Test Section for the Langley 0.3-Meter Transonic Cryogenic Tunnel. NASA Technical Paper 3049, Dec. 1990.

12. Rallo, Rosemary A.; Dress, David A.; and Siegle, Henry J.A.: Operating Envelope Charts for the Langley 0.3-Meter Transonic Cryogenic Wind Tunnel. NASA Technical Memorandum 89008, Aug. 1986.

13. Anon.: Gas Turbine Engine Inlet Flow Distortion. Society of Automotive Engineers Report ARP-1420, March 1978.

14. Buning, P.G., Jespersen, D.C., Pulliam, T.H., Klopfer, W.M., Chan, W.M., Slotnick, J.P., Krist, S.E., and Renze, K.J.: OVERFLOW User's Manual (Version 1.8m). 1999.

15. Jespersen, D.C., Pulliam, T.H., and Buning, P.G.: Vortex Generator Modeling for Navier-Stokes Codes. AIAA-97-0644, 1997.

16. Menter, F.: Improved Two-Equation Turbulence Model for Aerodynamic Flow. NASA Technical Memorandum 103975, 1992.

17. Chan, W.M., and Gomez, R.J.: Advances in Automatic Overset Grid Generation Around Surface Discontinuities. AIAA-02-3162.

18. Suhs, N.E., and Tramel, R.W.: PEGUSUS 4.0 User's Manual. AEDC-TR-91-8, Nov. 1991

19. Raymer, Daniel P.: Aircraft Design: A Conceptual Approach. Third Edition. AIAA Education Series. American Institute of Aeronautics and Astronautics, Inc., 1999.

20. Wellborn, S.R.; Reichert, B.A.; and Okiishi, T.H.: An Experimental Investigation of the Flow in a Diffusing S-Duct. AIAA-92-3622, 1992.

21. Little, B.H., Jr.; and Trimboli, W.S.: An Experimental Investigation of S-Duct Diffusers for High-Speed Prop-Fans. AIAA-82-1123, 1982.

22. Berrier, Bobby L.; and Morehouse, Melissa B.: Evaluation of Flush-Mounted, S-Duct Inlets With Large Amounts of Boundary Layer Ingestion. Research and Technology Agency Symposium on Vehicle Propulsion Integration. Warsaw, Poland. Paper No. 38, October 6-9, 2003.

TABLE 1.- Inlet geometry parameters.

	Inlets A & B	Inlets C & D
Aperture shape	semi-circular	semi-elliptical
Inlet throat design Mach number	0.7	0.7
Diffuser L/D_2	3.08	3.14
Inlet area ratio, A_2/A_h	1.069	1.056
Duct offset, $\Delta H/L$	0.337	0.314
Nominal δ/H_i	0.358	0.434

TABLE 2.- Nominal test conditions.

M	T_{T0}, °F	P_{T0}, psi	Re/ft	$Re_{,D2}$	$W2C/A_i$, lbm/s·ft^2	A0AH
0.25	-279	65	34 x 10^6	6.9 x 10^6	20.3 – 33.4	0.98 – 1.58
0.40	-279	62	51 x 10^6	10.4 x 10^6	20.3 – 33.8	0.64 – 1.06
0.60	-279	62	68 x 10^6	13.9 x 10^6	20.3 – 35.4	0.47 – 0.82
0.80	-279	52	68 x 10^6	13.9 x 10^6	20.3 – 35.8	0.40 – 0.72
0.83	-200	30	25 x 10^6	5.1 x 10^6	20.3 – 37.1	0.39 – 0.72
0.83	-200	36	30 x 10^6	6.1 x 10^6	20.3 – 37.1	0.39 – 0.72
0.83	-200	41	35 x 10^6	7.1 x 10^6	20.3 – 37.1	0.39 – 0.72
0.83	-200	50	42 x 10^6	8.6 x 10^6	20.3 – 37.1	0.39 – 0.72
0.83	-279	30	42 x 10^6	8.6 x 10^6	20.3 – 36.5	0.39 – 0.72
0.83	-279	40	57 x 10^6	11.6 x 10^6	20.3 – 36.5	0.39 – 0.72
0.83	-279	50	68 x 10^6	13.9 x 10^6	20.3 – 36.5	0.39 – 0.72

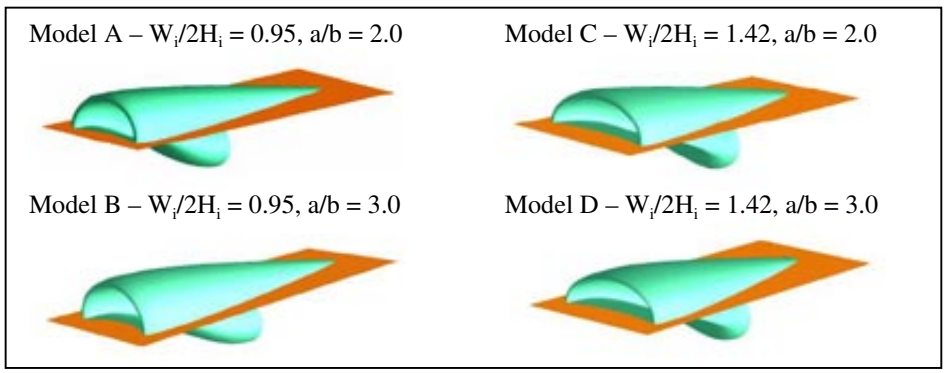

Figure 1.- Sketches showing 4 different inlet designs.

Figure 2.- Photograph of inlet model mounted on tunnel sidewall.

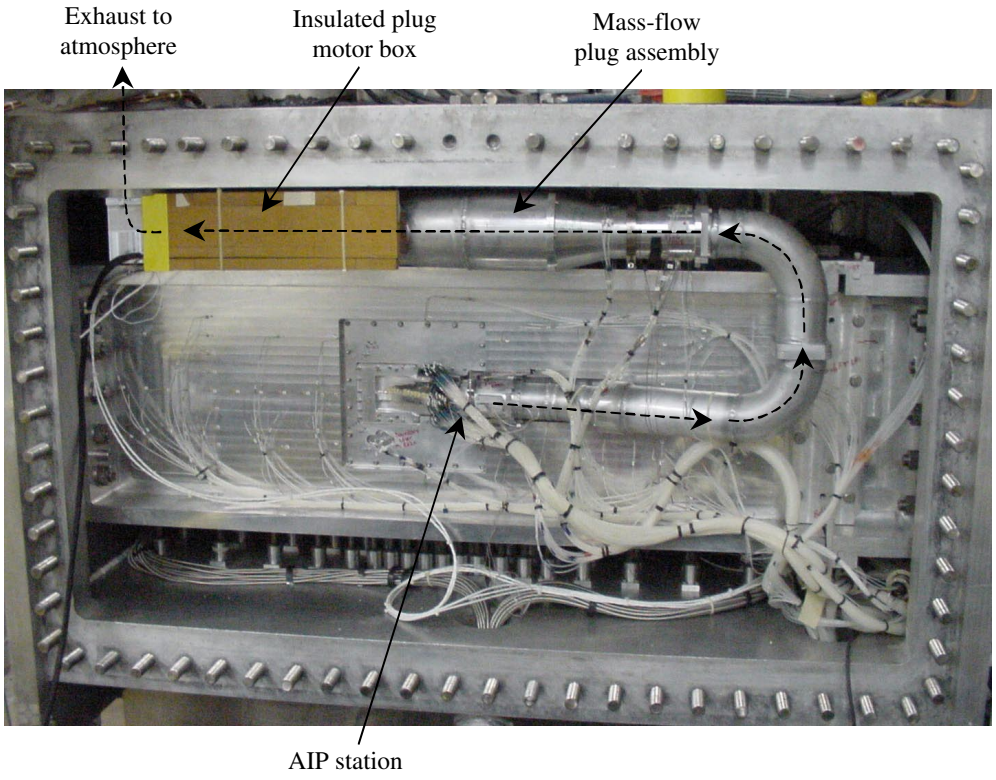

Figure 3.- Photograph showing inlet installation from backside of sidewall (tunnel plenum wall removed).

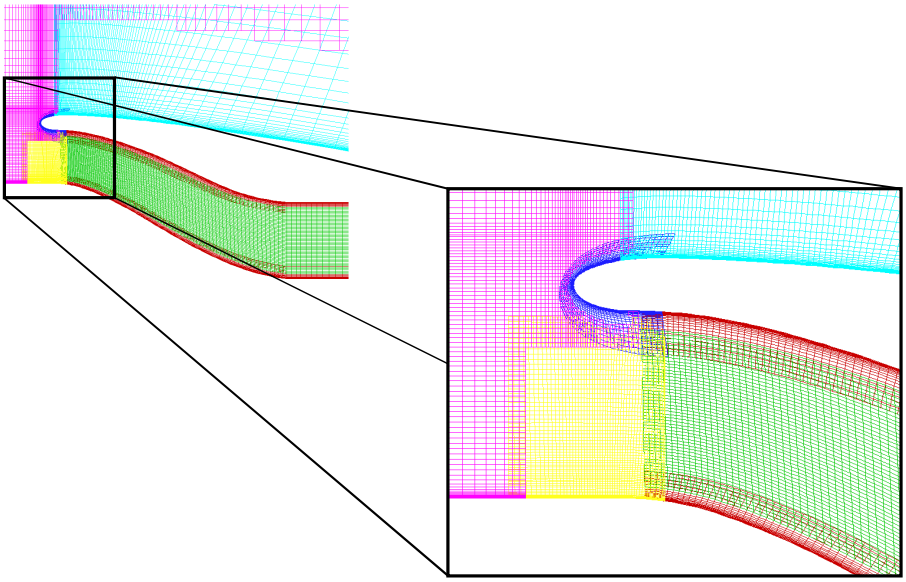

Figure 4.- Center plane view of the overset grids with a close-up of the inlet lip region.

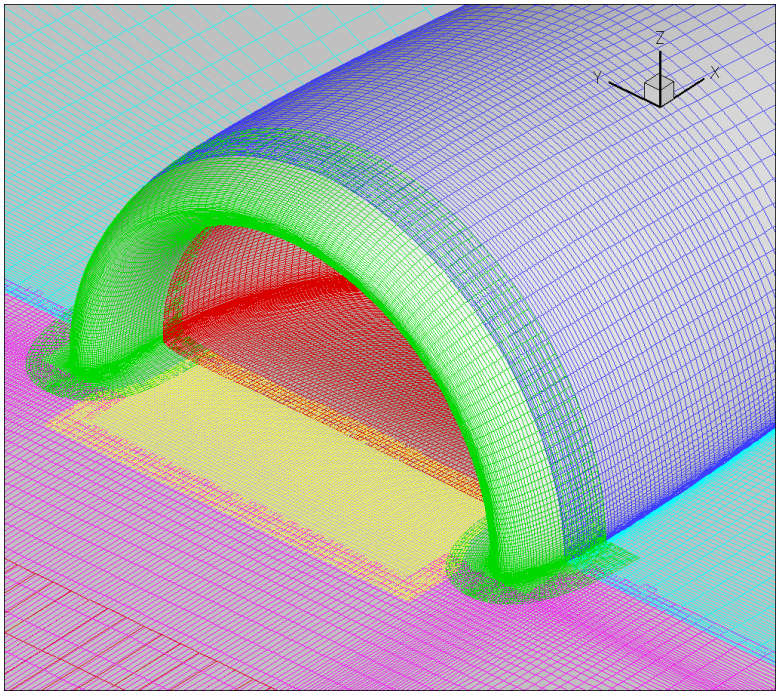

Figure 5.- Surface grids for inlet A

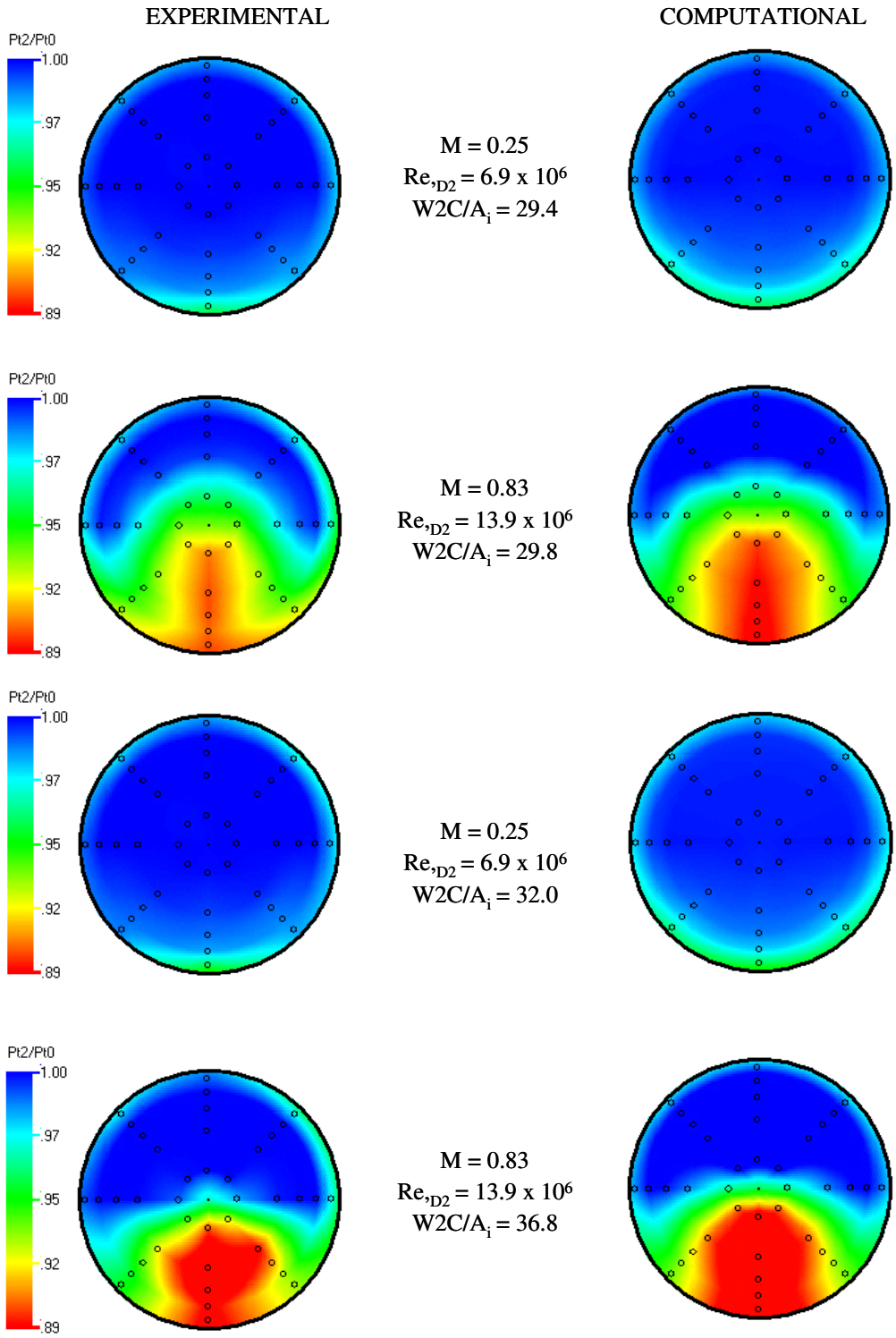

Figure 6.- Comparison of experimental and computational total-pressure contours for Inlet A.

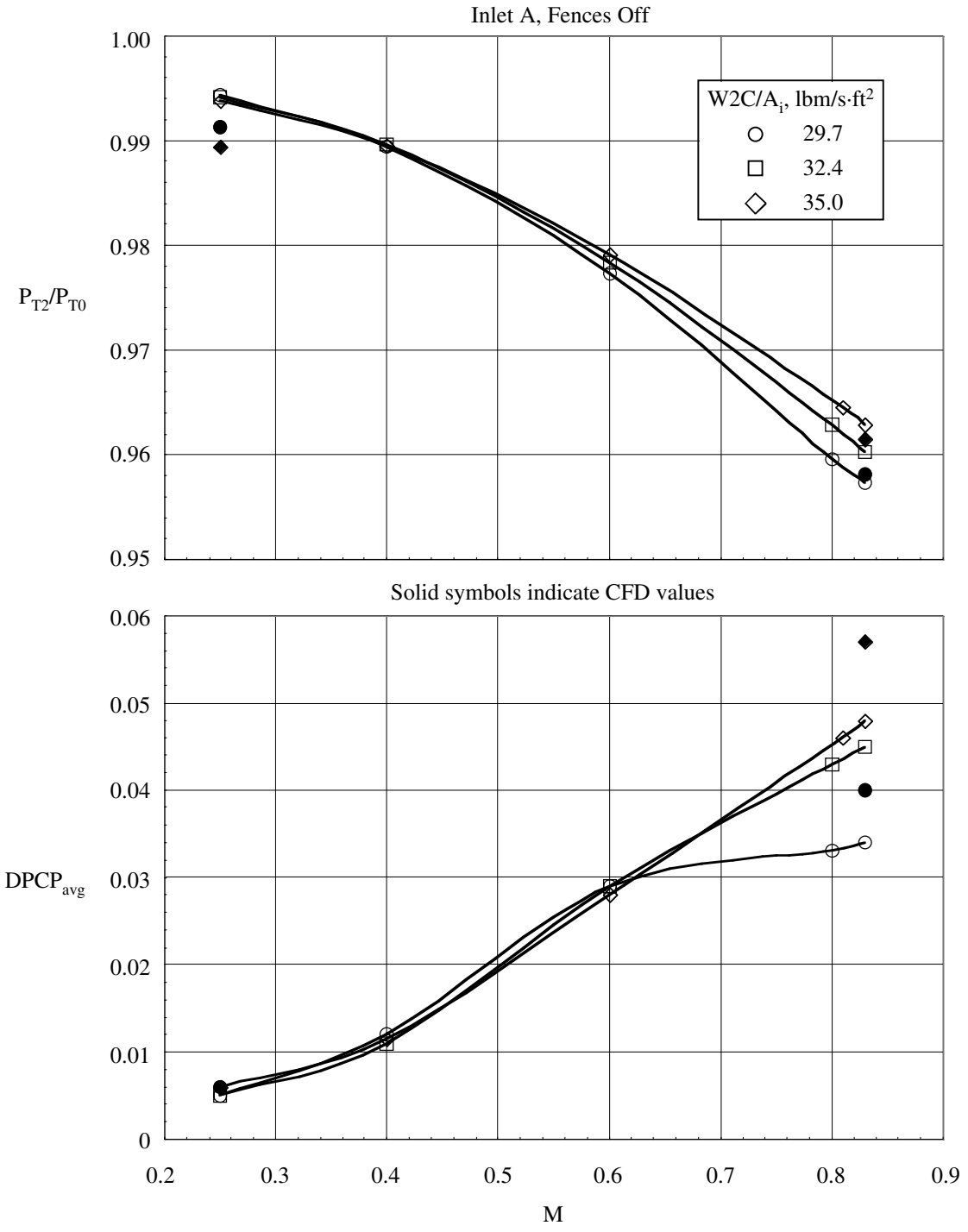

Figure 7.- Experimental and computational performance comparison of Inlet A.

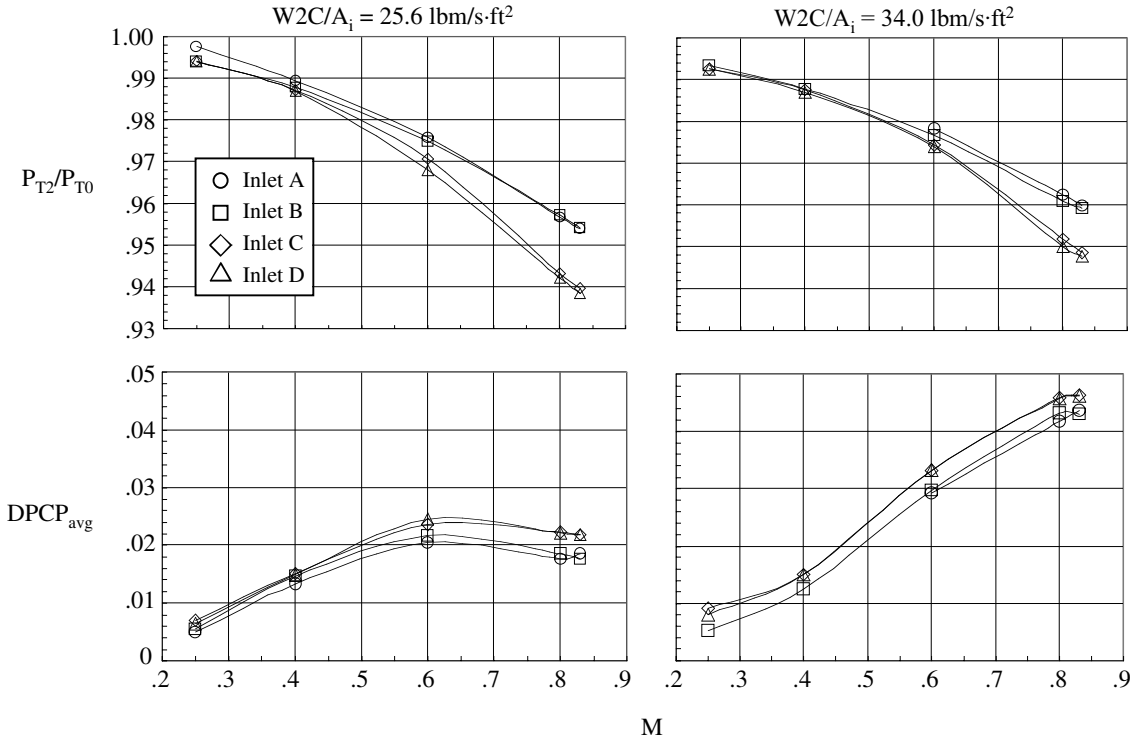

Figure 8.- Inlet performance comparison of Inlets A, B, C, and D.

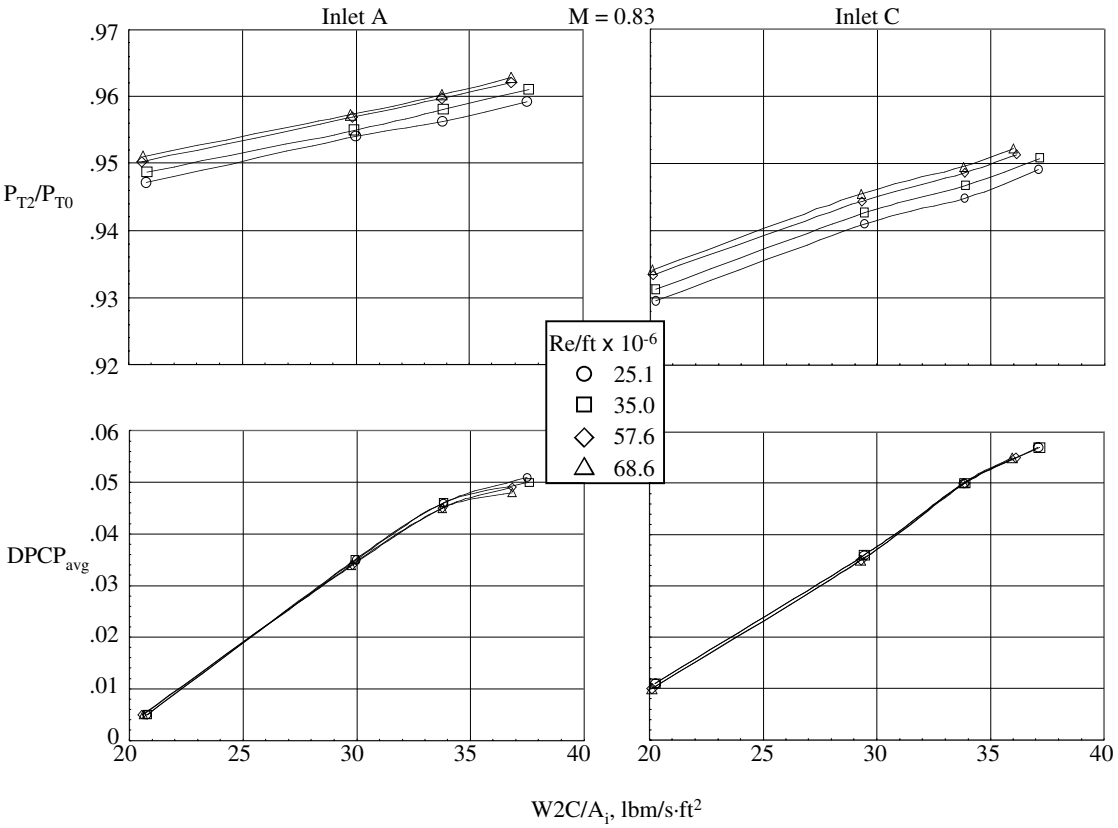

Figure 9.- Effect of Reynolds number on inlet performance at M = 0.83.

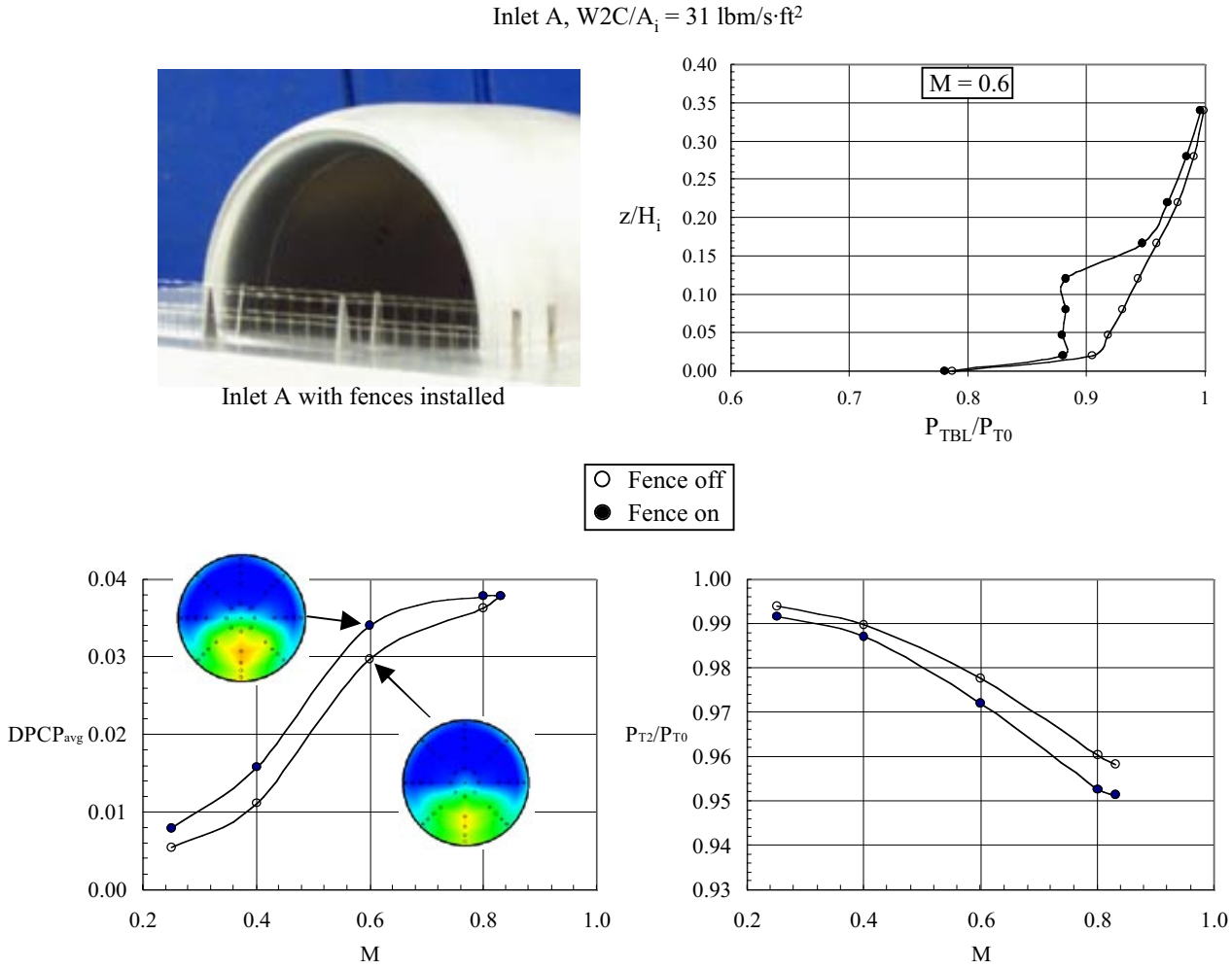

Figure 10.- Effect of a distorted entrance boundary layer profile on inlet performance. M = 0.6.